Statistical Properties of Electron Curtain Precipitation Estimated with AeroCube-6

M. Shumko[1,2], A.T. Johnson[1], T.P. O'Brien[3], D.L. Turner[4], A.D. Greeley[2], J.G. Sample[1], J.B. Blake[3], L.W. Blum[2], A.J. Halford[2]

[1]Department of Physics, Montana State University, Bozeman, Montana, USA
[2]NASA's Goddard Space Flight Center, Greenbelt, Maryland, USA
[3]Space Science Applications Laboratory, The Aerospace Corportation, El Segundo, California USA
[4]Johns Hopkins Applied Physics Laboratory, Laurel, Maryland, USA

Key Points:

- The dual AeroCube-6 CubeSats are used to identify stationary, narrow in latitude, and persistent > 30 keV precipitation termed curtains.
- 90% of the observed curtains in Low Earth Orbit are narrower than 20 kilometers in the latitudinal direction.
- Some curtains were continuously accelerated into the atmosphere for multiple seconds.

Corresponding author: M. Shumko, `msshumko@gmail.com`

Abstract

Curtains are a recently discovered stationary, persistent, and latitudinally narrow electron precipitation phenomenon in low Earth orbit. Curtains are observed over consecutive passes of the dual AeroCube-6 CubeSats while their in-track lag varied from a fraction of a second to 65 seconds, with dosimeters that are sensitive to > 30 keV electrons. This study uses the AeroCube-6 mission to quantify the statistical properties of 1,634 curtains observed over three years. We found that many curtains are narrower than 10 kilometers in the latitudinal direction with 90% narrower than 20 kilometers, corresponding to a few hundred kilometer radial size at the magnetic equator. We examined the magnetic local time and geomagnetic dependence of curtains. We found that curtains are observed in the late morning and midnight magnetic local times, with a higher occurrence rate at midnight, and curtains are observed more often during times of enhanced Auroral Electrojet. We found a few curtains in the bounce loss cone region above the north Atlantic, whose electrons were continuously scattered for at least 6 seconds as shown in one example. Such observations suggest that continuous curtain precipitation may be a significant loss of > 30 keV electrons from the magnetosphere into the atmosphere, possibly scattered by a parallel direct current electric field.

Plain Language Summary

Electron curtain precipitation from space into Earth's atmosphere is a recently-discovered phenomenon observed by dual-spacecraft missions such as the AeroCube-6 CubeSats that orbit 700 kilometers above Earth's surface. Curtains appear stationary, remaining unchanged from seconds to a minute. Curtains are also very narrow along the satellite orbit that is mostly in the latitudinal direction. Besides these two properties, curtains and their impact on the magnetosphere and atmosphere are not well understood. Therefore, we used the AeroCube-6 mission that took data together for three years, to statistically quantify curtain properties and to better understand their origin. We found 1,634 curtains and found that 90% of curtains are narrower than 20 kilometers in the latitudinal direction, curtains are observed on the outer radiation belt field lines, and curtains are observed when the magnetosphere is disturbed. Curtains observed in a special region above the North Atlantic shed light on their origin. A few dozen curtains observed in this North Atlantic region were continuously precipitating into the atmosphere for multiple seconds, and are unlikely to be drifting. Therefore, curtains may be a significant source of atmospheric ionization responsible for the natural depletion of ozone.

1 Introduction

Energetic particle precipitation into Earth's atmosphere plays a fundamental role in controlling the dynamics of Earth's radiation belts, and ionization of Earth's upper atmosphere (e.g. Millan & Thorne, 2007; Randall et al., 2015). Even though particle precipitation, and its impact on the magnetosphere and the atmosphere, has been extensively studied since the 1960s, there are precipitation phenomena that are still poorly understood. One such form of precipitation that we have limited knowledge of are electron curtains.

Electron curtain precipitation is a stationary phenomenon observed in low Earth orbit (LEO). Curtains are narrow in latitude and persist for up to a minute between subsequent satellite passes. They were recently discovered by Blake and O'Brien (2016) using the > 30 keV electron dosimeters onboard the dual AeroCube-6 (AC6) CubeSats that operated together between 2014 and 2017. This discovery was possible due to AC6's actively maintained in-track separation that varied between a few hundred meters and a few hundred kilometers. Besides the Blake and O'Brien (2016) study, not much is known about curtains including what they are, how are they generated, and their impact on the atmosphere. Answering these questions is an essential next step towards a more com-

plete understanding of how curtains, and particle precipitation in general, affect the magnetosphere and Earth's atmosphere.

In low Earth orbit, curtains are narrower than a few tens of kilometers in the latitudinal direction. A polar-orbiting LEO satellite, such as AC6, will pass through their cross-section in a few seconds; curtains appear in the electron count time series as short enhancements in flux. AC6 also observes similar-looking transient precipitation called electron microbursts. Curtains and microbursts are observed in the AC6 data but appear short-lived for different reasons: microbursts are temporal, while curtains are spatial. Hence AC6, and other recently developed multi-spacecraft missions, are necessary to identify and distinguish between the transient microbursts precipitation and the persistent curtain precipitation.

Since the mid-1960s, microbursts have been observed by high altitude balloons where they appear as sharp peaks in flux with a sub-second duration (e.g. Anderson & Milton, 1964; R. Brown et al., 1965; Parks, 1967). Because balloons are relatively stationary, a microburst is easily classified as a transient phenomenon. Microburst electrons have also been directly observed by LEO satellites such as The Solar Anomalous and Magnetospheric Particle Explorer (e.g. Blake et al., 1996; Lorentzen, Blake, et al., 2001; O'Brien et al., 2003; Douma et al., 2017). But precipitation that looks like a microburst from a single LEO satellite is ambiguous—it can be transient, stationary and narrow in latitude, or both. Thus, multi-spacecraft missions such as the Focused Investigations of Relativistic Electron Burst Intensity, Range, and Dynamics (FIREBIRD-II) (Crew et al., 2016; Johnson et al., 2020) and AC6 (Blake & O'Brien, 2016; O'Brien et al., 2016) are necessary to resolve the temporal vs. spatial ambiguity. While this study focuses on curtain precipitation, microburst precipitation observed by AC6 was studied in Shumko et al. (2020).

While the impact of curtains on the magnetosphere and Earth's atmosphere is unknown, the impact of microbursts has been estimated to be substantial. Lorentzen, Looper, and Blake (2001), Thorne et al. (2005), Breneman et al. (2017), and Douma et al. (2019), among others, estimated that microbursts could deplete the outer radiation belt electrons in about a day. Furthermore, Seppälä et al. (2018) modeled a 6-hour microburst storm and concluded that microbursts depleted mesospheric ozone by roughly 10%. Microbursts and narrow curtains can be easily misidentified from a single spacecraft; if curtains are numerous, then the atmospheric and magnetospheric impact associated with microburst observations from single satellites may be overestimated.

Blake and O'Brien (2016) proposed a hypothesis that curtains are drifting remnants of microbursts. If a microburst is not completely lost in the atmosphere after the initial scatter, the remaining microburst electrons will spread out (bounce phase disperse) along the entire magnetic field line over a few bounce periods. Concurrently these electrons drift to the east, with higher energy electrons drifting at a faster rate. Assuming this hypothesis, the initially localized microburst is also spread out in longitude into the shape of a curtain. A similar phenomena was hypothesized by Lehtinen et al. (2000) who predicted that drifting curtains can be created by energetic runaway beams driven by lightning, but these curtains will be observed at relatively low L shells.

Precipitation bands, sometimes also referred to as spikes (e.g. Imhof et al., 1991), is another form of precipitation that can be related to curtains. Precipitation bands are stationary and were observed to persist from an hour to as much as half a day (e.g. J. Brown & Stone, 1972; Blake et al., 1996). Blum et al. (2013) identified two precipitation bands and estimated that only 20 precipitation bands can deplete the outer radiation belt electrons. The mechanism responsible for scattering precipitation band electrons at high L is believed to be field line curvature scattering, but the scattering mechanism for band electrons at lower L shells. A few proposed scattering mechanisms include wave-particle

interactions and acceleration due to a parallel direct current potential (Hoffman & Evans, 1968).

This study expands on Blake and O'Brien (2016) by examining the statistical properties of curtains. We use 1634 confirmed curtain observations to study the distributions of the curtain: width in latitude, the geomagnetic conditions favorable to curtains, and the curtain distribution in L and magnetic local time (MLT). Lastly we will show examples of curtains that continuously precipitated in the bounce loss cone (BLC) region.

2 Instrumentation

The AC6 mission was a pair of 0.5U (10x10x5 cm) CubeSats built by The Aerospace Corporation and designed to measure the electron and proton environment in low Earth orbit (O'Brien et al., 2016). AC6 was launched on 19 June 2014 into a 620x700 km, 98° inclination orbit. The AC6 orbit over the three year mission lifetime was roughly dawn-dusk, and precessed only a few hours in MLT: 8-12 MLT in the dawn and 20-24 MLT in the dusk sectors. The two AC6 spacecraft, designated as AC6-A and AC6-B, separated after launch and were in proximity for the duration of the three-year mission—maintained by an active attitude control system. The attitude control system allowed them to actively control the amount of atmospheric drag experienced by each AC6 unit using the surface area of their solar panel "wings." By changing their orientation, AC6 was able to maintain a separation between 2-800 km, confirmed by the Global Positioning System. The two AC6 units were in a string of pearls configuration, so one unit, typically unit A, was leading the other by an in-track lag: the time it would take the following spacecraft to catch up to the position of the leading spacecraft. To convert between the AC6 in-track separation and in-track lag, the AC6 orbital velocity was used. AC6's orbital velocity was 7.6 km/s and varied by as much as 0.1 km/s. The in-track lag is readily available in the data files with the Global Positioning System, which makes it possible to remove the spatiotemporal ambiguity that affects single-spacecraft measurements.

Each AC6 unit contains three Aerospace microdosimeters (licensed to Teledyne Microelectronics, Inc) that measure the electron and proton dose in orbit (O'Brien et al., 2016). The dosimeter used for this study is dos1 with a > 30 keV integral electron response, as the other dosimeters either responded primarily to protons or were not identical between unit A and B. All dosimeters sample at 1 Hz in survey mode, and 10 Hz in burst mode. 10 Hz data was readily available from both AC6 units from June 2014 to May 2017 while their in-track lag was less than 65 seconds. Figure A1 shows the distribution of 10 Hz data as a function of AC6 in-track lag. The variety of AC6 separations and data availability over the three-year mission makes it possible to study transient electron microburst precipitation (Shumko et al., 2020) and now stationary electron curtain precipitation.

3 Methodology

3.1 Curtain Identification

The 10 Hz data were used to identify curtains using the following two criteria: a high spatial correlation, and a prominent peak. Before we applied the identification criteria, the AC6-B time series was shifted by the in-track lag to spatially align it with the AC6-A time series.

The first identification criterion is a 1-second rolling Pearson correlation applied to both time series. Spatial features with a correlation greater than 0.8 are considered highly correlated. The second criterion is applied to the highly correlated features to check if they are also prominently peaked. To find peaked precipitation, we used a similar technique to the technique used by Blum et al. (2015) to identify precipitation bands, and

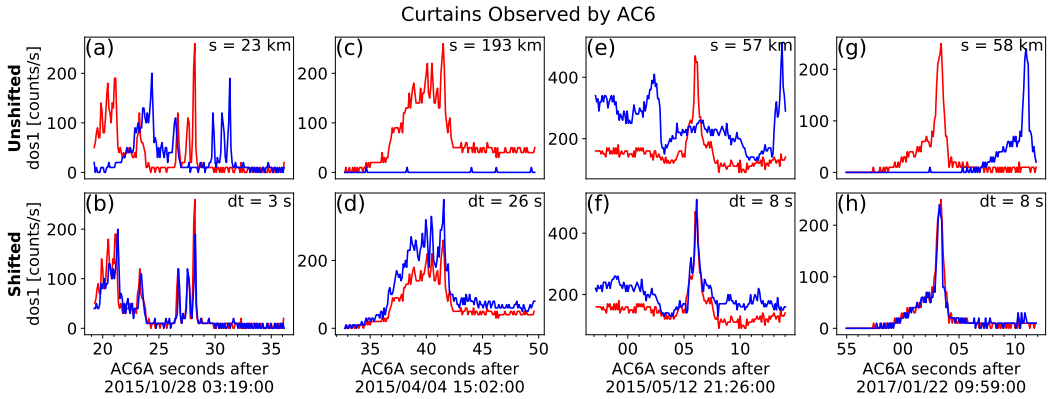

Figure 1. Four examples showing the > 30 keV electron time series data taken by AC6 at the same time (unshifted) in the top row and at the same position (shifted by dt seconds) in the bottom row. AC6-A, whose data is shown with the red curves, was s kilometers ahead of AC6-B. To show the data at the same position the AC6-B time series was shifted by the in-track lag annotated by dt. These examples show that curtain precipitation was highly correlated for up to 26 seconds.

by Greeley et al. (2019) to identify microbursts. Our technique quantified the number of Poisson standard deviations, σ, that dos1 counts (counts in each 100 ms bin) are above a 10-second centered running average, b_{10}. Locations where dos1 counts are at least two σ above b_{10}, in other words $dos1 > 2\sqrt{b_{10}} + b_{10}$, are considered prominently peaked. One bias inherent to this detection algorithm, and similar algorithms such as the burst parameter (O'Brien et al., 2003), is a reduced sensitivity for wider peaks. For curtains with a width similar to b_{10}, the baseline will be elevated making the curtain peak less pronounced.

We tuned the automated detection parameters to identify a large number of curtains while reducing the number of false positive detections. Once curtains were automatically identified, one author visually inspected 6,149 every candidate curtain and verified 1,634 curtains. The visual inspection was performed to remove false positive detections that were triggered by: sharp count rate shoulders, low baseline (b_{10}), and unrealistically high correlations resulting from Poisson noise. Four curtain examples are shown in Fig. 1. In each instance, the unmodified time series is shown in the top row and the spatially-aligned time series in the bottom row. The in-track lag used to shift the bottom row is annotated by dt, corresponding to an AC6 in-track separation annotated by s. The bottom row shows highly correlated curtains observed at the same location for at least 3 to 26 seconds.

3.2 Differentiating Between Drifting and Precipitating Curtains

The AC6 dosimeters lack the necessary pitch angle resolution to differentiate between locally drifting and precipitating electrons to test the Blake and O'Brien (2016) hypothesis that curtains are the drifting remnants of microbursts. Fortunately, one standard method of distinguishing between locally precipitating, drifting, and trapped particles is by using the geographic location of observations with respect to the location of the South Atlantic Anomaly (SAA).

Earth's magnetic field is asymmetric and has a region of weaker magnetic field in the South Atlantic Ocean called the South Atlantic Anomaly. The weaker magnetic field in the SAA naturally differentiates particles by pitch angle into trapped and quasi-trapped

populations. While some particles observed in LEO are trapped and will execute closed drift paths, most particles observed in LEO are quasi-trapped: they drift around the Earth until they reach the SAA. Within the SAA, the weaker magnetic field strength can lower the particle's mirror point altitude into the atmosphere, where collisions with the atmospheric neutrals and ions are more numerous and the particle is lost.

Particles that are quasi-trapped have pitch angles in the drift loss cone and will precipitate within one drift period (often within the SAA) (e.g. Selesnick et al., 2003). Particles with smaller equatorial pitch angles that are lost in the atmosphere within one bounce are in the bounce loss cone (BLC). Traditionally, a particle is in the BLC if its mirror point altitude is at or below 100 km in either hemisphere (e.g. Selesnick et al., 2003).

In most regions outside of the SAA and its conjugate point in the North Atlantic, AC6 will observe a combination of drift and bounce loss cone electrons. In the SAA, AC6 does not only observe electrons that are immediately lost, but a combination of electrons that are in the drift loss cone, bounce loss cone, and trapped (a trapped electron that locally mirrors at AC6's altitude in the SAA will mirror at higher altitudes everywhere else). In the region magnetically conjugate to the SAA in the North Atlantic, AC6 only observes electrons in the BLC. Here, if an electron makes it to AC6's altitude, it might be in the local loss cone and precipitate in the local hemisphere. Alternatively, the electron may mirror at or below AC6 and bounce to its conjugate mirror point deep in the atmosphere or below sea level in the SAA. Therefore, any electrons observed in the BLC region will likely precipitate within one bounce (≈ 1.5 seconds for 30 keV electrons).

We estimated the BLC region for locally-mirroring electrons in the North Atlantic Ocean using the IRBEM-Lib magnetic field library and the Olson-Pfitzer magnetic field model (Boscher et al., 2012; Olson & Pfitzer, 1982). We defined a latitude-longitude grid, with a $\approx 0.5^\circ \times 0.5^\circ$ grid size, spanning the North Atlantic at 700-kilometers altitude, and estimated the local magnetic field strength. The 700-kilometers altitude was chosen because it is the upper bound altitude for AC6's orbit and it is the conservative limit because at lower altitudes the BLC region is larger. For each latitude-longitude point we traced the magnetic field line to the southern hemisphere and found the conjugate mirror point altitude. If the conjugate mirror point is ≤ 100 kilometers, the electron is likely lost and the associated grid point is considered to be in the BLC. Furthermore, a more rigorous bounce loss cone criterion is the conjugate mirror point altitude below sea level. In this case, the electron is likely lost. Since AC6 can measure locally-mirroring electrons in the North Atlantic, the spacecraft altitude determines the upper bound conjugate mirror point altitude in the SAA. The BLC region estimated by this method closely matches the BLC region shown in Comess et al. (2013, Figure 1) and Dietrich et al. (2010, Figure 3) for other LEO satellites. Furthermore, we repeated the same analysis using the Tsyganenko 1989 model (Tsyganenko, 1989), which yielded similar boundaries.

4 Results

In this study we addressed three questions: what is the distribution of curtain widths along the AC6 orbit (mostly in geographic latitude), when and where are curtains observed, and are curtains due to drifting or locally precipitating?

4.1 Curtain Width

The curtain width is quantified as the width at half of the curtain's topographic prominence that is described in Appendix B. The spatial width of a curtain is then the product of the observed width in time and AC6's orbital velocity. The curtain width is measured along AC6's orbit track which is mostly in the north-south direction, therefore the estimated curtain widths are also mostly in the north-south direction. The dis-

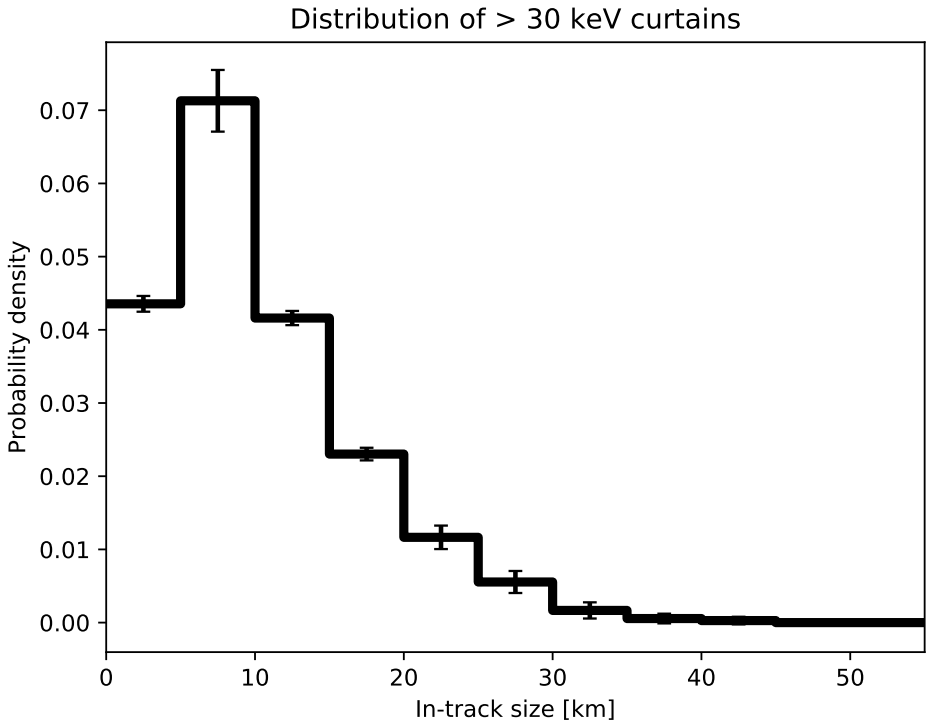

Figure 2. The distribution of curtain width in latitude. The error bars are derived assuming the Poisson standard error.

tribution of curtain widths is shown in Fig. 2. Curtains are very narrow. Many curtains are narrower than 10 km in latitude, and 90% are narrower than 20 km in latitude.

4.2 When and Where Are Curtains Observed

The distribution of curtains in L and MLT is shown in Fig. 3. Figure 3a shows the distribution of the observed curtains while Fig. 3b shows the same distribution normalized by the number of quality 10 Hz samples (flag = 0 in the data files) that AC6 took at the same location in each L-MLT bin. In Fig. 3a and 3b, the bins with where no curtains were observed are white. The AC6 sampling distribution is shown in Fig. 3c, whose white bins show where AC6 did not take any 10 Hz data at the same location. The normalized curtain distribution in Fig. 3b shows an enhanced curtain occurrence in the outer radiation belt with the largest peak in the pre-midnight MLT sector.

We also examine the geomagnetic conditions favorable for curtains. Figure 4a shows the distribution of the minute cadence Auroral Electroject (AE) index between 2014 and 2017 in solid black, for times when quality dos1 data were available from both AC6 units. Furthermore, the distribution of the AE index when curtains were observed is shown by the solid blue lines. Curtains are observed during both low and high geomagnetic activity, slightly more often at higher AE than the idex itself (curtain distribution trends above the AE index when $AE > 200$). Lastly, we normalized the curtain distribution in Fig. 4a assuming any AE index is equally probable. The normalized curtain distribution is shown in Fig. 4b, which emphasizes that the curtain occurrence frequency increases with increasing AE index.

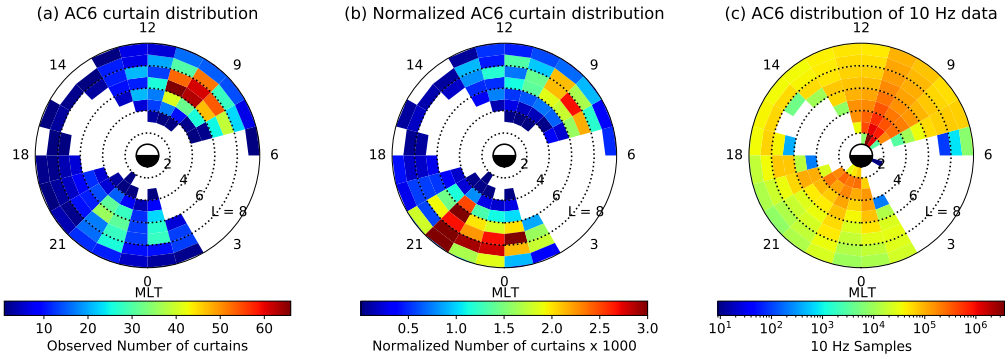

Figure 3. The distribution of observed curtains by L shell and MLT. Panel a shows the locations of all observed curtains used in this study. Panel b shows the curtain distribution normalized by the number of quality 10 Hz samples taken in each bin, shown in panel c. The white bins in panels a and b show where no curtains were observed. In panel c the white bins show where AC6 did not take any 10 Hz data at the same location.

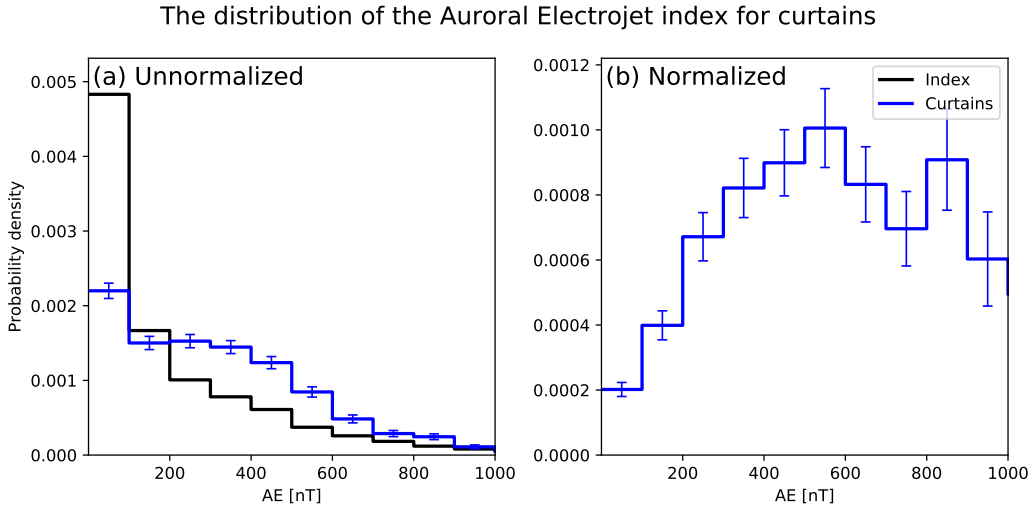

Figure 4. The distribution of the Auroral Electroject (AE) index when curtains were observed. The blue line in panel a shows the distribution of AE when curtains where observed, and for reference the black line is shows the distribution of the entire AE index between 2014 and 2017 when quality 10 Hz data is available from both AC6 spacecraft. Panel b shows the curtain distribution normalized by the AE index distribution, and it represents the distribution assuming that any AE index is equally probable. The error bars are derived assuming the Poisson standard error.

4.3 Local Atmospheric Precipitation

Lastly we investigate if curtains are drifting or locally precipitating. Figure 5a shows a map of the northern BLC region in the North Atlantic. The solid blue line is the northern boundary where an electron that mirrors locally at 700 km has a conjugate mirror point at 100 km in the SAA. Immediately south of the solid blue line, the conjugate mirror altitude rapidly decreases towards, and below, sea level. The dashed blue line is the boundary where the conjugate mirror point altitude is at sea level. South of this line the conjugate mirror point is inside the Earth. For reference, AC6 takes about 30 seconds to move between the solid and dashed blue curves. The two dotted black curves in Fig. 5a are roughly the boundary of the outer radiation belt, defined as $L = 4 - 8$.

Of the 1634 curtains, we found 36 curtains that were observed inside the BLC region. Figure 5b-e shows 4 curtain examples (AC6-B time shifted by the in-track lag), along with the AC6 in-track lag, L and MLT during the observations annotated. The AC6 locations where these curtains were observed are shown in Fig. 5a with the red stars and the corresponding panel labels.

5 Discussion

5.1 Curtain Width

Curtains are narrow in latitude. Figure 2 shows that the width of most curtains is on the order of $1 - 3$ seconds in time as observed by AC6, correspoding to a $8 - 20$ kilometer spatial width along the AC6 orbit track. Scaled to the magnetic equator, these widths correspond to a source with a radial scale size of a few hundred kilometers. The reduced sensitivity of the detection algorithm, as described in Section 3.1, is unlikely to significantly underestimate the curtain width distribution because most curtains had a width less than half of the 10-second baseline's width.

As shown in Fig. 1, it is remarkable that some curtains maintain a fine and narrow structure after multiple seconds with little observable difference. However, sometimes curtains appear to be slightly and systematically shifted in latitude, while maintaining their fine structure (not shown).

5.2 When and Where Are Curtains Observed

Figure 3b shows that curtains likely originate in the outer radiation belt and are observed relatively more in the pre-midnight than late-morning MLT regions. Furthermore, curtains are likely observed at higher L shells near midnight MLT, however the sampling statistics at high L are limited because AC6 rapidly crosses high L shells. Nevertheless, Fig. 3b hints that curtains near midnight MLT were observed at L shells possibly outside the outer radiation belt. Lastly, Figure 4b shows that curtains are associated with an enhanced AE.

5.3 Curtains Observed in The Bounce Loss Cone

The handful of curtains observed in the bounce loss cone, and shown in Fig. 5, put the Blake and O'Brien (2016) curtain drift hypothesis into question. These curtains were observed near the sea level mirror altitude curve. One possible explanation is that the drifting curtain electrons were observed at the end of their drift orbit, however because these examples were seen far from the western edge of the BLC, any drifting electrons would have been lost before AC6 observed them. Thus, they were not drifting and were precipitating for as long as 6 seconds, as shown in Fig. 5e. The curtain precipitation persisted for multiple bounce periods (≈ 1.5 seconds for 30 keV electrons in this region). There are relatively few mechanisms capable of persistently scattering electrons. The scat-

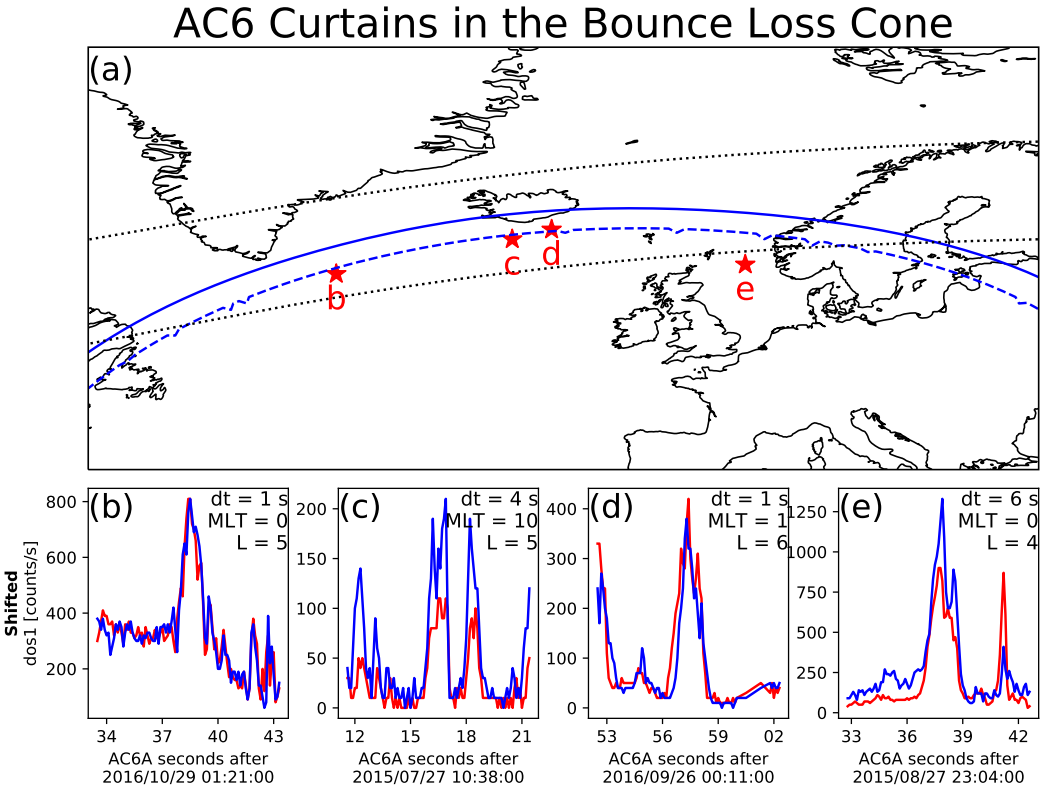

Figure 5. Curtains observed in the bounce loss cone region. Panel a shows a map of the North Atlantic region with the outer radiation belt, defined by $L = 4 - 8$, shown with the dotted black curves. The solid blue curve shows the northern boundary of the bounce loss cone region. Along this curve, electrons locally mirroring at 700 kilometers altitude have a conjugate mirror point at 100 kilometers altitude in the SAA. A more strict bounce loss cone criterion is the dashed blue curve that represents a conjugate mirror point altitude at sea level in the SAA. The 4 red stars with labels show the locations of the curtain examples shown in the corresponding panels b-e. The panels b-e show the 4 example curtains with the AC6-A data shown by the red line and the time-shifted AC6-B data with the blue line. The annotations in each example show the AC6 in-track lag (dt), L, and MLT rounded to the nearest integer. AC6-A was ahead in all examples except in panel d.

tering mechanism must be radially localized; if we assume the mechanism is at the magnetic equator, it must be on a scale of a few hundred kilometers. One candidate mechanism is a direct current electric field that is parallel to the background magnetic field that lowers the electron mirror point to AC6 altitudes. To find the minimum potential we assume the electron is barely trapped and has a 100-kilometer conjugate mirror point altitude in the SAA, so initially the electron will mirror above AC6 in the bounce loss cone region.

To find the parallel potential, $q\Phi$, we use the kinetic energy, W, of a 30 keV electron at its initial mirror point with a magnetic field strength of B_i. The kinetic energy at the initial mirror point can be written as $W_i = \mu B_i$ where μ is the first adiabatic invariant that is conserved during this acceleration. When a parallel potential acts on the electron of charge q and does $q\Phi$ amount of work, the electron will mirror closer to Earth's surface and mirror at a field strength B_f where its final energy is $W_f = \mu B_f$. Now we relate the initial and final kinetic energy of the electron,

$$\mu B_f = \mu B_i + q\Phi. \tag{1}$$

Then we solve for $q\Phi$ and substitute μ to express the above equation as a function of the initial kinetic energy

$$q\Phi = W_i \frac{(B_f - B_i)}{B_i}. \tag{2}$$

The parallel potential is proportional to W_i so a larger potential is necessary to accelerate higher energy electrons. AC6 dos1 electron energy response increases rapidly from 30 keV to a peak at 100 keV (Figure 2 in O'Brien et al., 2019), therefore our assumption that $W_i = 30$ keV can underestimate the parallel potential. However, the counts observed by AC6 are a convolution of, among other things, the AC6 dos1 electron energy response and the falling electron energy spectrum. Thus, the majority of electrons that AC6 observed have energies close to 30 keV and the $W_i = 30$ is an appropriate approximation.

We again used IRBEM-Lib to estimate $q\Phi$. For each example curtain in Fig. 5, we first estimated the local magnetic field, B_f, that the electron descended to after the acceleration. Then we traced the local field line into the SAA. We estimated B_i at 100 kilometers altitude in the SAA for barely trapped electrons. With the initial and final B, along with $W = 30$ keV, the minimum potential was between $q\Phi = 1 - 4$ kV for the examples shown in Fig. 5.

The range of estimated potentials is typical for the inverted-V discrete aurora. Partamies et al. (2008) used the observations made by the Fast Auroral SnapshoT (FAST) mission. They reported that the auroral inverted-V electron precipitation structures, with electron energies up to a few tens of keV, were accelerated by 2-4 kV parallel potentials. The inverted-V structure and curtains share several similarities including: latitudinal width, high occurrence rate in the midnight MLT region, and the maximum inverted-V energy extends into tens of keV (e.g. Marklund et al., 2011; Thieman & Hoffman, 1985). AC6's dos1, with its 30 keV electron threshold, may by observing the highest energy tip of the inverted-V aurora. A possible connection between the inverted-V structures is intriguing, but by itself AC6 cannot easily test this hypothesis. To investigate further, a follow-on study could look at ground-based auroral imager data and look for meso-scale auroral arcs when AC6 observed curtains overhead.

Regardless of the source of the curtain precipitation, the impact of curtains on the atmosphere needs to be quantified. Even if the curtains observed in the BLC are the exception and other curtains are drifting, the drifting curtains will still precipitate within one drift period. Precipitating electrons produce odd reactive nitrogen (NO_X) molecules

that are currently underestimated by atmospheric models such as the widely-used Whole Atmosphere Community Climate Model (WACCM) (e.g. Randall et al., 2015). Curtain precipitation could explain the lack of atmospheric odd Nitrogen. However, an AC6-like mission with pitch angle and energy resolution will be necessary to quantify the curtain impact on the atmosphere.

6 Conclusions

The 1,634 curtains examined here allowed us to make the following inferences:

1. Curtains are narrow—90% are less than 20 kilometers wide in latitude.
2. Curtains are observed predominately in the pre-midnight MLT region, and during active geomagnetic periods.
3. Some curtains continuously precipitate into the atmosphere for multiple seconds.

As shown in Fig. 1, curtain precipitation is narrow with a fine structure that persists for multiple seconds: for at least 26 seconds as shown in Fig. 1d. Either the scattering mechanism that continuously generates curtains is physically static for multiple seconds, or the curtain electron drift is often undisturbed.

The curtain-microburst relationship hypothesized in Blake and O'Brien (2016) is not clear. Curtains observed in the bounce loss cone cast doubt on the curtain-microburst hypothesis. Some curtains continuously precipitate for at least a few seconds, and can be a significant source of energetic electron precipitation into the atmosphere. Lastly, we found that the continuous scattering of curtain electrons can be explained by a parallel direct current electric field, possibly relating curtains to the aurora.

Appendix A Distribution of Colocated 10 Hz Data

Figure A1 shows the distribution of colocated AC6 10 Hz data as a function of in-track lag. This distribution is heavily dominated by small in-track lags and 72% of the colocated 10 Hz data was taken when AC6 was separated in-track by less than 10 seconds, corresponding to 75 km in-track separation. Therefore, most of the curtains studied here were observed for small in-track lags, which limits our ability to explore the extent of curtain duration.

Appendix B Estimating Curtain Widths

The curtain width in the dos1 time series is defined here as the width at half of the curtain's topographic prominence. Topographic prominence for a peak in a time series is the height of a peak relative to the maximum of the two minima on either side of the peak. The minima on either side of the peak are searched for between the peak and the nearest higher peak on that side. Figure B1 shows 5 examples of curtains observed by AC6A in red (for clarity the AC6B data is not shown), and the curtain width is shown by the horizontal black line.

Acknowledgments
This work was made possible with the help from the many engineers and scientists at The Aerospace Corporation who designed, built, and operated AC6. M. Shumko was supported by NASA Headquarters under the NASA Earth and Space Science Fellowship Program - Grant 80NSSC18K1204 and NASA Postdoctoral Program at the NASA's Goddard Space Flight Center, administered by Universities Space Research Association under contract with NASA. D.L. Turner is thankful for funding from a NASA grant (prime award #: 80NSSC19K0280). The work at The Aerospace Corporation was supported

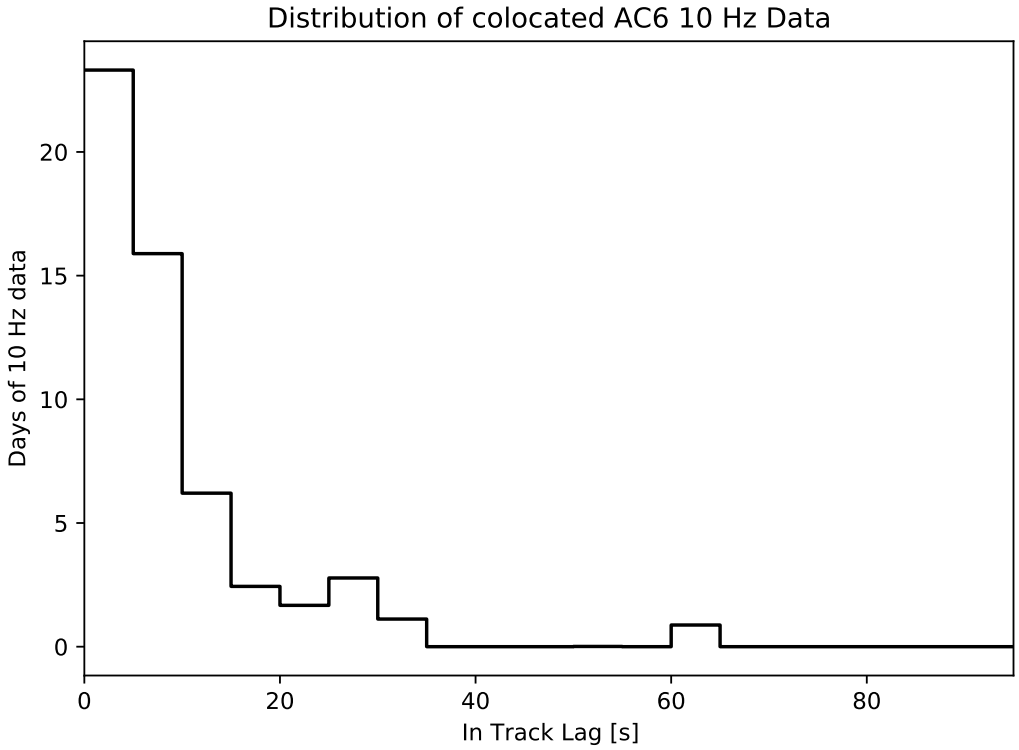

Figure A1. The distribution of colocated 10 Hz data as a function of in-track lag. Bins are 5 kilometers wide.

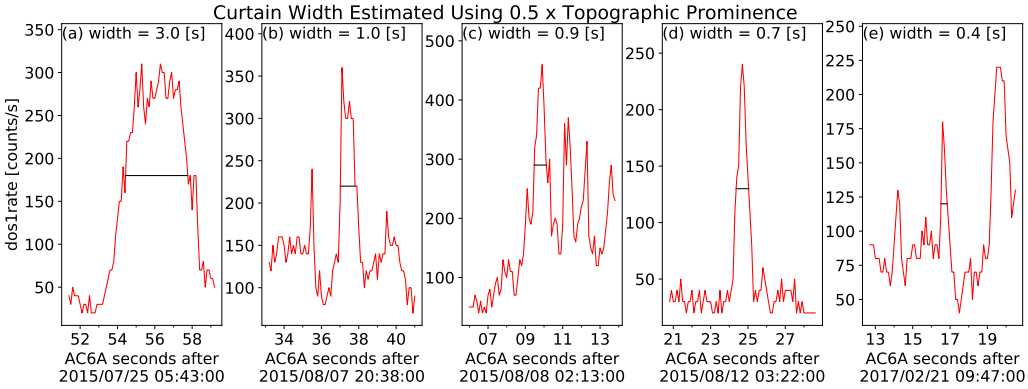

Figure B1. Five examples of curtains observed by AC6A shown with the red curves and the curtain widths are shown with the horizontal black lines. The height of the horizontal black lines are at half of the curtain's topographic prominence.

in part by RBSP-ECT funding provided by JHU/APL contract 967399 under NASA's Prime contract NAS501072. The AC6 data and documentation is available at http://rbspgway.jhuapl.edu/ac6 and the IRBEM-Lib version used for this analysis can be downloaded from https://sourceforge.net/p/irbem/code/616/tree/.

References

Anderson, K. A., & Milton, D. W. (1964). Balloon observations of X rays in the auroral zone: 3. High time resolution studies. *Journal of Geophysical Research*, *69*(21), 4457–4479. Retrieved from http://dx.doi.org/10.1029/JZ069i021p04457 doi: 10.1029/JZ069i021p04457

Blake, J. B., Looper, M. D., Baker, D. N., Nakamura, R., Klecker, B., & Hovestadt, D. (1996). New high temporal and spatial resolution measurements by sampex of the precipitation of relativistic electrons. *Advances in Space Research*, *18*(8), 171 - 186. Retrieved from http://www.sciencedirect.com/science/article/pii/0273117795009698 doi: http://dx.doi.org/10.1016/0273-1177(95)00969-8

Blake, J. B., & O'Brien, T. P. (2016). Observations of small-scale latitudinal structure in energetic electron precipitation. *Journal of Geophysical Research: Space Physics*, *121*(4), 3031–3035. Retrieved from http://dx.doi.org/10.1002/2015JA021815 (2015JA021815) doi: 10.1002/2015JA021815

Blum, L., Li, X., & Denton, M. (2015). Rapid MeV electron precipitation as observed by SAMPEX/HILT during high-speed stream-driven storms. *Journal of Geophysical Research: Space Physics*, *120*(5), 3783–3794. Retrieved from http://dx.doi.org/10.1002/2014JA020633 (2014JA020633) doi: 10.1002/2014JA020633

Blum, L., Schiller, Q., Li, X., Millan, R., Halford, A., & Woodger, L. (2013). New conjunctive cubesat and balloon measurements to quantify rapid energetic electron precipitation. *Geophysical research letters*, *40*(22), 5833–5837.

Boscher, D., Bourdarie, S., O'Brien, P., Guild, T., & Shumko, M. (2012). *Irbem-lib library*.

Breneman, A., Crew, A., Sample, J., Klumpar, D., Johnson, A., Agapitov, O., ... others (2017). Observations directly linking relativistic electron microbursts to whistler mode chorus: Van allen probes and FIREBIRD II. *Geophysical Research Letters*.

Brown, J., & Stone, E. (1972). High-energy electron spikes at high latitudes. *Journal of Geophysical Research*, *77*(19), 3384–3396.

Brown, R., Barcus, J., & Parsons, N. (1965, 6). Balloon observations of auroral zone x rays in conjugate regions. 2. microbursts and pulsations. *Journal of Geophysical Research (U.S.)*, *70*. doi: 10.1029/JZ070i011p02599

Comess, M., Smith, D., Selesnick, R., Millan, R., & Sample, J. (2013). Duskside relativistic electron precipitation as measured by sampex: A statistical survey. *Journal of Geophysical Research: Space Physics*, *118*(8), 5050-5058. Retrieved from https://agupubs.onlinelibrary.wiley.com/doi/abs/10.1002/jgra.50481 doi: 10.1002/jgra.50481

Crew, A. B., Spence, H. E., Blake, J. B., Klumpar, D. M., Larsen, B. A., O'Brien, T. P., ... Widholm, M. (2016). First multipoint in situ observations of electron microbursts: Initial results from the NSF FIREBIRD II mission. *Journal of Geophysical Research: Space Physics*, *121*(6), 5272–5283. Retrieved from http://dx.doi.org/10.1002/2016JA022485 (2016JA022485) doi: 10.1002/2016JA022485

Dietrich, S., Rodger, C. J., Clilverd, M. A., Bortnik, J., & Raita, T. (2010). Relativistic microburst storm characteristics: Combined satellite and ground-based observations. *Journal of Geophysical Research: Space Physics*, *115*(A12).

Douma, E., Rodger, C., Blum, L., O'Brien, T., Clilverd, M., & Blake, J. (2019).

Characteristics of relativistic microburst intensity from sampex observations. *Journal of Geophysical Research: Space Physics*.

Douma, E., Rodger, C. J., Blum, L. W., & Clilverd, M. A. (2017). Occurrence characteristics of relativistic electron microbursts from SAMPEX observations. *Journal of Geophysical Research: Space Physics*, *122*(8), 8096–8107. Retrieved from http://dx.doi.org/10.1002/2017JA024067 (2017JA024067) doi: 10.1002/2017JA024067

Greeley, A., Kanekal, S., Baker, D., Klecker, B., & Schiller, Q. (2019). Quantifying the contribution of microbursts to global electron loss in the radiation belts. *Journal of Geophysical Research: Space Physics*.

Hoffman, R. A., & Evans, D. S. (1968). Field-aligned electron bursts at high latitudes observed by ogo 4. *Journal of Geophysical Research*, *73*(19), 6201–6214.

Imhof, W., Voss, H., Mobilia, J., Datlowe, D., & Gaines, E. (1991). The precipitation of relativistic electrons near the trapping boundary. *Journal of Geophysical Research: Space Physics*, *96*(A4), 5619–5629.

Johnson, A., Shumko, M., Griffith, B., Klumpar, D., Sample, J., Springer, L., ... others (2020). The FIREBIRD-II CubeSat mission: Focused investigations of relativistic electron burst intensity, range, and dynamics. *Review of Scientific Instruments*, *91*(3), 034503.

Lehtinen, N. G., Inan, U. S., & Bell, T. F. (2000). Trapped energetic electron curtains produced by thunderstorm driven relativistic runaway electrons. *Geophysical research letters*, *27*(8), 1095–1098.

Lorentzen, K. R., Blake, J. B., Inan, U. S., & Bortnik, J. (2001). Observations of relativistic electron microbursts in association with VLF chorus. *Journal of Geophysical Research: Space Physics*, *106*(A4), 6017–6027. Retrieved from http://dx.doi.org/10.1029/2000JA003018 doi: 10.1029/2000JA003018

Lorentzen, K. R., Looper, M. D., & Blake, J. B. (2001). Relativistic electron microbursts during the GEM storms. *Geophysical Research Letters*, *28*(13), 2573–2576. Retrieved from http://dx.doi.org/10.1029/2001GL012926 doi: 10.1029/2001GL012926

Marklund, G. T., Sadeghi, S., Cumnock, J. A., Karlsson, T., Lindqvist, P.-A., Nilsson, H., ... others (2011). Evolution in space and time of the quasi-static acceleration potential of inverted-v aurora and its interaction with alfvénic boundary processes. *Journal of Geophysical Research: Space Physics*, *116*(A1).

Millan, R., & Thorne, R. (2007). Review of radiation belt relativistic electron losses. *Journal of Atmospheric and Solar-Terrestrial Physics*, *69*(3), 362 - 377. Retrieved from //www.sciencedirect.com/science/article/pii/S1364682606002768 doi: http://dx.doi.org/10.1016/j.jastp.2006.06.019

O'Brien, T. P., Blake, J. B., & W., G. J. (2016, May). *AeroCube-6 dosimeter data README* (Tech. Rep. No. TOR-2016-01155). The Aerospace Corporation.

O'Brien, T. P., Looper, M. D., & Blake, J. B. (2019, July). *AeroCube-6 dosimeter equivalent energy thresholds and flux conversion factors* (Tech. Rep. No. TOR-2017-02598). The Aerospace Corporation.

O'Brien, T. P., Lorentzen, K. R., Mann, I. R., Meredith, N. P., Blake, J. B., Fennell, J. F., ... Anderson, R. R. (2003). Energization of relativistic electrons in the presence of ULF power and MeV microbursts: Evidence for dual ULF and VLF acceleration. *Journal of Geophysical Research: Space Physics*, *108*(A8). Retrieved from http://dx.doi.org/10.1029/2002JA009784 doi: 10.1029/2002JA009784

Olson, W. P., & Pfitzer, K. A. (1982). A dynamic model of the magnetospheric magnetic and electric fields for july 29, 1977. *Journal of Geophysical Research: Space Physics*, *87*(A8), 5943–5948. Retrieved from http://dx.doi.org/10.1029/JA087iA08p05943 doi: 10.1029/JA087iA08p05943

Parks, G. K. (1967). Spatial characteristics of auroral-zone X-ray microbursts. *Jour-*

nal of Geophysical Research, *72*(1), 215–226.

Partamies, N., Donovan, E., & Knudsen, D. (2008). Statistical study of inverted-v structures in fast data. In *Annales geophysicae* (Vol. 26, pp. 1439–1449).

Randall, C. E., Harvey, V. L., Holt, L. A., Marsh, D. R., Kinnison, D., Funke, B., & Bernath, P. F. (2015). Simulation of energetic particle precipitation effects during the 2003–2004 arctic winter. *Journal of Geophysical Research: Space Physics*, *120*(6), 5035–5048.

Selesnick, R. S., Blake, J. B., & Mewaldt, R. A. (2003). Atmospheric losses of radiation belt electrons. *Journal of Geophysical Research: Space Physics*, *108*(A12). Retrieved from http://dx.doi.org/10.1029/2003JA010160 (1468) doi: 10.1029/2003JA010160

Seppälä, A., Douma, E., Rodger, C., Verronen, P., Clilverd, M. A., & Bortnik, J. (2018). Relativistic electron microburst events: Modeling the atmospheric impact. *Geophysical Research Letters*, *45*(2), 1141–1147.

Shumko, M., Johnson, A., Sample, J., Griffith, B. A., Turner, D. L., O'Brien, T. P., ... Claudepierre, S. G. (2020). Electron microburst size distribution derived with AeroCube-6. *Journal of Geophysical Research: Space Physics*, e2019JA027651.

Thieman, J. R., & Hoffman, R. A. (1985). Determination of inverted-v stability from dynamics explorer satellite data. *Journal of Geophysical Research: Space Physics*, *90*(A4), 3511–3516.

Thorne, R. M., O'Brien, T. P., Shprits, Y. Y., Summers, D., & Horne, R. B. (2005). Timescale for MeV electron microburst loss during geomagnetic storms. *Journal of Geophysical Research: Space Physics*, *110*(A9). Retrieved from http://dx.doi.org/10.1029/2004JA010882 (A09202) doi: 10.1029/2004JA010882

Tsyganenko, N. (1989). A solution of the chapman-ferraro problem for an ellipsoidal magnetopause. *Planetary and Space Science*, *37*(9), 1037 - 1046. Retrieved from http://www.sciencedirect.com/science/article/pii/0032063389900767 doi: http://dx.doi.org/10.1016/0032-0633(89)90076-7